Naval Research Laboratory

Washington, DC 20375-5320

NRL/FR/5320--95-9780

An Azimuth Measurement Algorithm for Mechanically Rotating Pulse Doppler Radars

GREGORY TAVIK
BEN CANTRELL

Advanced Radar Systems Branch
Radar Division

June 15, 1995

REPORT DOCUMENTATION PAGE

Form Approved
OMB No. 0704-0188

1. AGENCY USE ONLY (*Leave Blank*)	2. REPORT DATE	3. REPORT TYPE AND DATES COVERED
	June 15, 1995	

4. TITLE AND SUBTITLE

An Azimuth Measurement Algorithm for Mechanically Rotating Pulse Doppler Radars

5. FUNDING NUMBERS

PE - 64755N

6. AUTHOR(S)

Gregory Tavik and Ben Cantrell

7. PERFORMING ORGANIZATION NAME(S) AND ADDRESS(ES)

Naval Research Laboratory
Washington, DC 20375-5320

8. PERFORMING ORGANIZATION REPORT NUMBER

NRL/FR/5320--95-9780

9. SPONSORING/MONITORING AGENCY NAME(S) AND ADDRESS(ES)

Program Executive Office (Theater Air Defense)
2531 Jefferson Davis Highway
Arlington, VA 22217-5000

10. SPONSORING/MONITORING AGENCY REPORT NUMBER

11. SUPPLEMENTARY NOTES

Submitted to *IEEE Aerospace and Electronic Systems*

12a. DISTRIBUTION/AVAILABILITY STATEMENT

Approved for public release; distribution unlimited.

12b. DISTRIBUTION CODE

13. ABSTRACT (*Maximum 200 words*)

For a mechanically rotating pulse Doppler radar having only a single main beam, an algorithm is presented that obtains an estimate of a target's azimuth angle using echo data obtained over a single coherent dwell. By removing the clutter and then cross-correlating the target echoes with a stored replica of the antenna pattern, azimuth angle measurement accuracies can be obtained within a fraction of a beamwidth. A Monte Carlo simulation was performed to determine the measurement error as a function of Signal-to-Noise Ratio (SNR) and target angular location within the radar's main beam.

14. SUBJECT TERMS

Pulse Doppler radar
Antenna Scan
Modulation Target Azimuth
Measurement

15. NUMBER OF PAGES

14

16. PRICE CODE

17. SECURITY CLASSIFICATION OF REPORT	18. SECURITY CLASSIFICATION OF THIS PAGE	19. SECURITY CLASSIFICATION OF ABSTRACT	20. LIMITATION OF ABSTRACT
UNCLASSIFIED	UNCLASSIFIED	UNCLASSIFIED	UL

CONTENTS

AN AZIMUTH MEASUREMENT ALGORITHM FOR MECHANICALLY ROTATING PULSE DOPPLER RADARS

INTRODUCTION

Mechanically rotating pulse Doppler radars need very accurate measurements of a target's range, radial velocity, and azimuth to maintain accurate tracks. For a mechanically rotating pulse Doppler radar having only a single main beam, greater azimuth angle measurement accuracies may be obtained by using the amplitude modulation of the echoes caused by the rotating antenna pattern. By using this property, measurement accuracies on the order of a fraction of a (3 dB) beamwidth are expected on a single coherent dwell. This report describes the algorithm for obtaining the azimuth estimate and presents some expected errors obtained by computer simulation.

BACKGROUND

In a pulse Doppler radar, multiple pulses are transmitted at a high rate to measure the relative phase change from pulse to pulse due to the Doppler shift caused by a moving target. Since low-velocity clutter has a different Doppler shift than high-speed targets, the high-speed targets can be detected in the presence of clutter. This is illustrated with the aid of Fig. 1, which shows an example of an ambiguity diagram plotted with range on the x-axis, Doppler (velocity) on the y-axis, and signal power on the z-axis. Figure 1 shows clutter at all ranges for very low values of Doppler and at the Pulse Repetition Frequency (PRF) (corresponding to high values of Doppler), as well as a single target and a thermal noise floor.

The ambiguity diagram is formed as follows. The time interval that the radar beam dwells on a target is often called the Coherent Dwell Interval (CDI). During a CDI, a certain number of pulses is transmitted at a constant PRF. After the echoes have reached a steady state condition, echoes from the last N pulses are processed. After conversion to baseband (by using a synchronous in-phase/quadrature detector), the echoes within each Pulse Repetition Interval (PRI) are sampled and digitized at a slightly higher rate (sufficient to avoid aliasing) than the instantaneous radar bandwidth to obtain a complex received waveform. These N complex sampled waveforms are arranged side-by-side and a fast Fourier transform (FFT) is taken across the N pulses for each range cell. In this way, the data are transformed from the "pulse domain" (or time domain at a certain range cell) to the "Doppler domain" and Fig. 1 is obtained.

AZIMUTH MEASUREMENT ALGORITHM

The azimuth measurement algorithm takes advantage of the fact that the antenna pattern amplitude modulates the N echoes from the target as the beam scans past it. This received signal having the antenna pattern modulation imposed on it can then be cross-correlated with the previously stored replica of the antenna's main lobe pattern. The angle associated with the maximum value of the cross-correlation function provides the estimated angle of arrival of the received signal for the isolated target. Figure 2 is

Manuscript approved May 8, 1995.

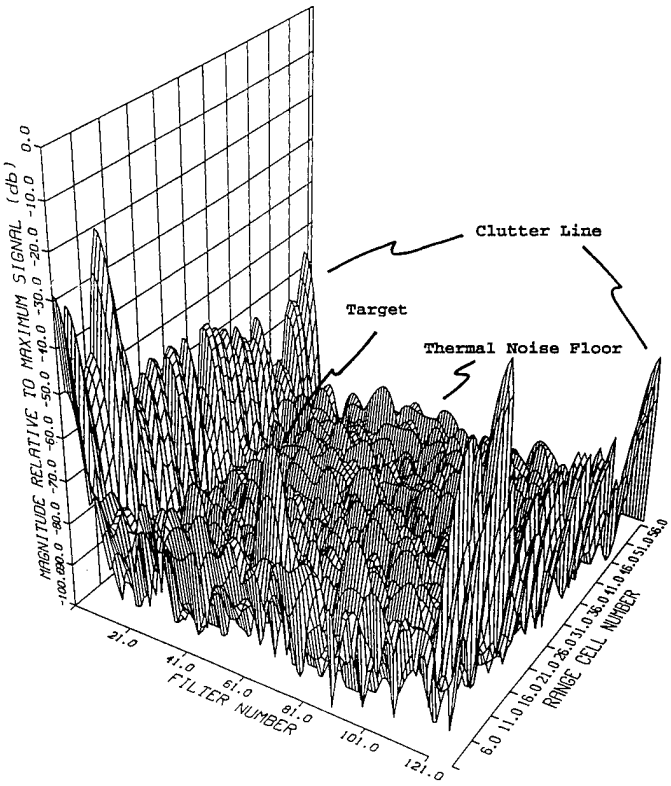

Fig. 1 — Ambiguity diagram containing clutter, target, and thermal noise

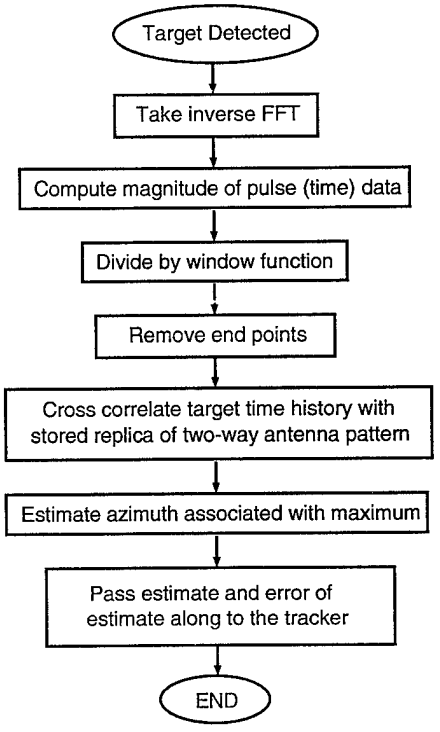

Fig. 2 — Flow diagram of the azimuth measurements algorithm using data from the range cell in which the target is detected

a flow diagram of the algorithm. The diagram assumes that an ambiguity diagram has been formed for the CDI, the clutter line has been filtered (or zeroed) out, a threshold has been applied, and a target has been detected at a certain range cell. It is at this point that the algorithm begins. Figure 3 shows an example of the Doppler domain power spectrum for a single range cell before the clutter has been filtered out. The clutter is centered on the lowest and highest Doppler bins, or filters (which correspond to 0 and 2π phase change).

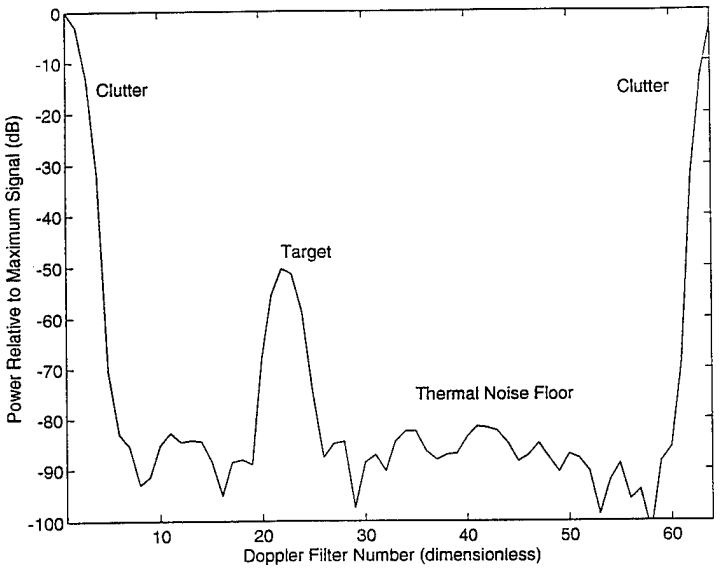

Fig. 3 — Single range cell of ambiguity diagram containing clutter, target, and thermal noise

After zeroing the clutter, the sampled complex Doppler space containing the target signal is transformed back to the pulse domain with an inverse FFT. The magnitude of the signal is found and then divided by the windowing function that was applied before the FFT. This yields an approximation to the amplitude weighting due to the antenna scan modulation. A few endpoints are removed because they are badly corrupted by the distortion introduced by zeroing the clutter with a "brick wall" notch filter. This leaves M samples, where $M < N$. This distortion could be reduced by implementing a more sophisticated notch filter. Using the data from Fig. 3, these operations produce the result shown in Fig. 4.

At this point, the data is cross-correlated with a stored replica of the radar's antenna pattern. It is assumed that the antenna pattern is well known out to at least the first few sidelobes. The antenna pattern sampling interval θ_s, given in degrees, is determined by

$$\theta_s = \alpha_{ant} \times t_{PRI} , \tag{1}$$

where α_{ant} is the antenna's angular scan rate in degrees per second and t_{PRI} is the pulse repetition interval in seconds.

The cross correlation function γ_k is given by

$$\gamma_k = \frac{s^T a_k}{\sqrt{s^T s} * \sqrt{a_k^T a_k}} , \tag{2}$$

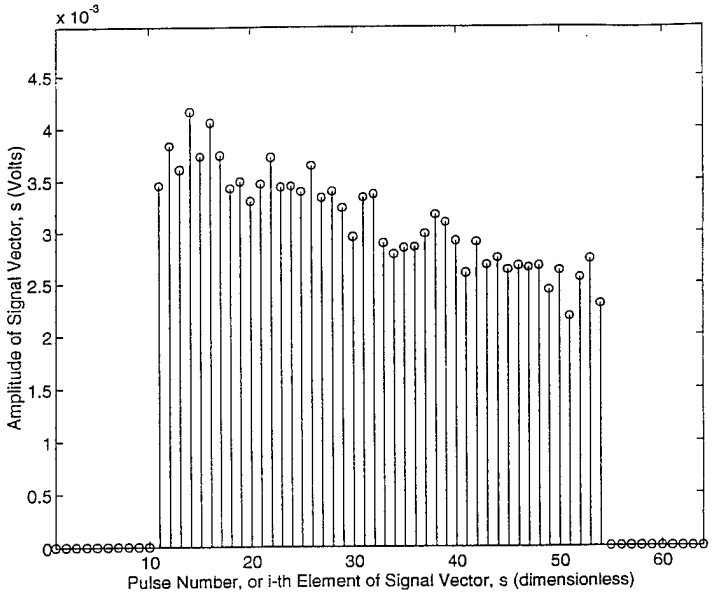

Fig. 4 — Magnitude of the target signal s after the clutter was removed in the Doppler domain, the inverse FFT was applied, and the remaining signal was divided by the windowing function. (The distorted endpoints have been removed.)

where s is an M dimensional vector containing the return signal's magnitude, and a_k is an M dimensional vector containing a replica of the antenna pattern delayed by k [1]. Using the data in Fig. 4 for s and the antenna pattern shown in Fig. 5 to generate a_k, Eq. (2) produces the K cross-correlator outputs shown in Fig. 6. The index k^*, which is associated with the maximum value of the cross correlation function, can be used to derive the corresponding azimuth estimate θ_{est} by

$$\theta_{est} = \left[k^* - \frac{K}{2} \right] \times \theta_s + \theta_{ant} , \tag{3}$$

where the first term on the right-hand side represents an offset angle from the average center position of the main beam θ_{ant} during the CDI.

SIMULATION RESULTS

A Monte Carlo simulation was conducted to determine the measurement errors. Table 1 shows the values of the constants and functions used in this simulation. Figures 7 and 8 show the root-mean-squared (RMS) error and Figs. 9 and 10 show the standard deviation of the azimuth estimate as a function of true target azimuth offset measured from the center of the beam and Signal-to-Noise Ratio (SNR) calculated *after* integration. Both the error and the target location relative to the center of the beam shown in Figs. 7 through 10 are provided in terms of fractions of a (one-way) 3 dB beamwidth.

Each data point is calculated using 100 different complex, white Gaussian noise sequences generated with Matlab's "randn" pseudo-random normal number generator. Figures 11 and 12 show the probability of the estimate to be within 0.3 of the one-way 3 dB beamwidth, which in this case is $0.3 \times 125° = 0.375°$. These figures show that once the post-integration SNR reaches 35 dB, angle estimate errors are less than a third of a beamwidth.

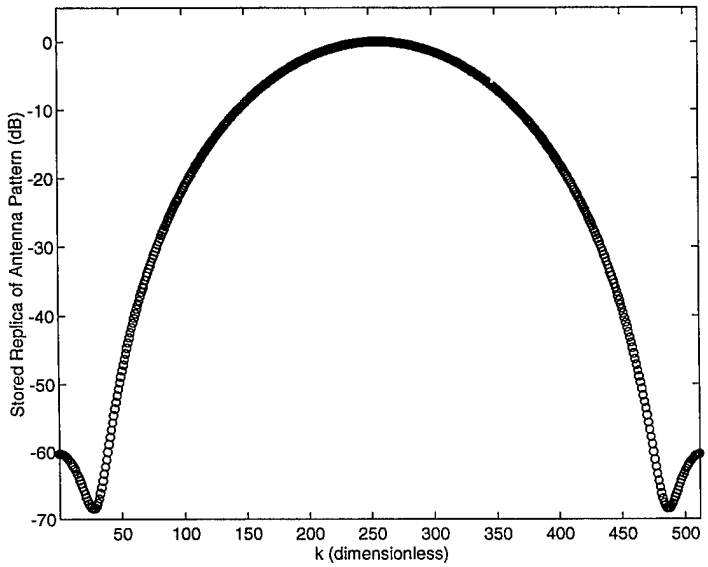

Fig. 5 — Antenna two-way main lobe beam pattern samples. The antenna sampling interval θ_s = 0.00714°, so that the main lobe beamwidth is 3.7°.

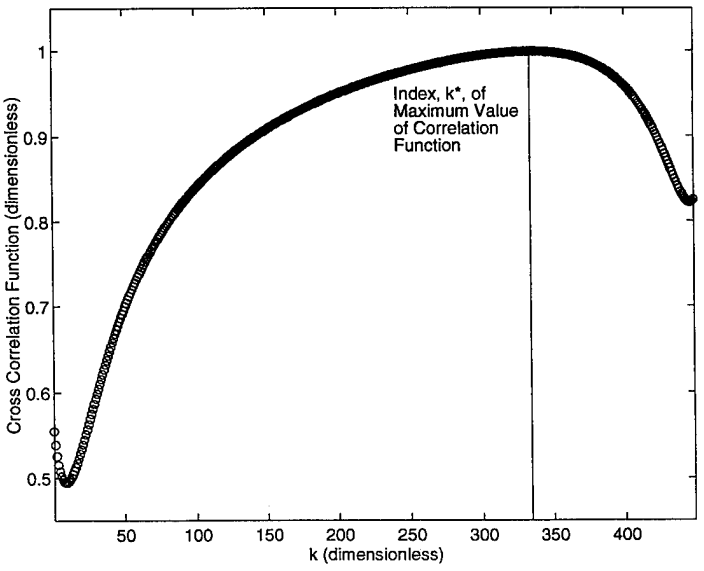

Fig. 6 — Output of antenna pattern cross correlator γ_k using the target signal in Fig. 4 and the stored replica of the two-way antenna pattern in Fig. 5

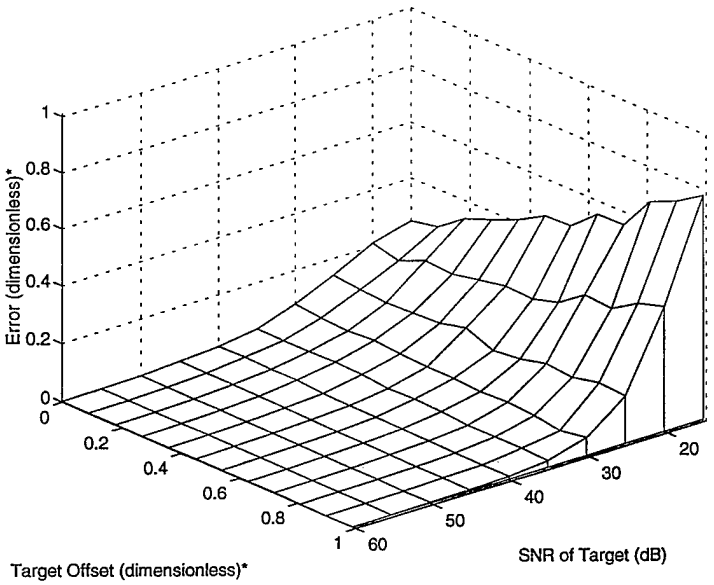

Fig. 7 — RMS error of azimuth estimate (*target offset and error are measured in fractions of a 3 dB beamwidth)

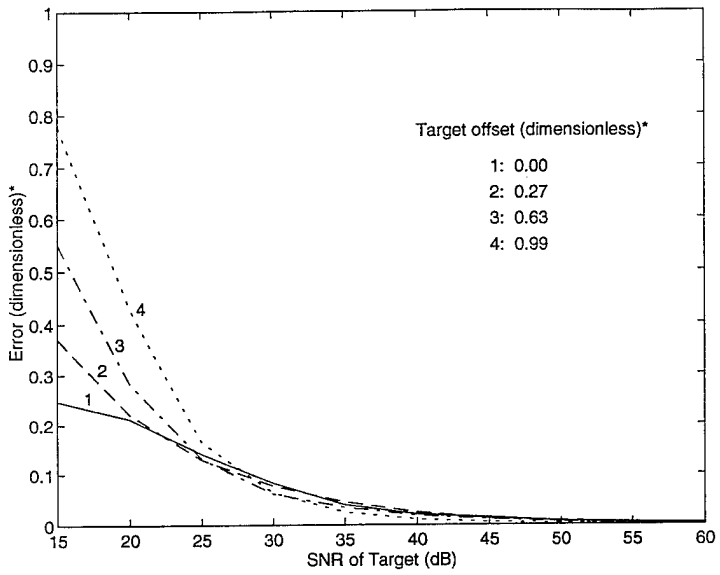

Fig. 8 — RMS error of azimuth estimate. These four curves have been extracted from Fig. 7 and plotted here for further clarity. (*Target offset and error are measured in fractions of a one-way 3 dB beamwidth.)

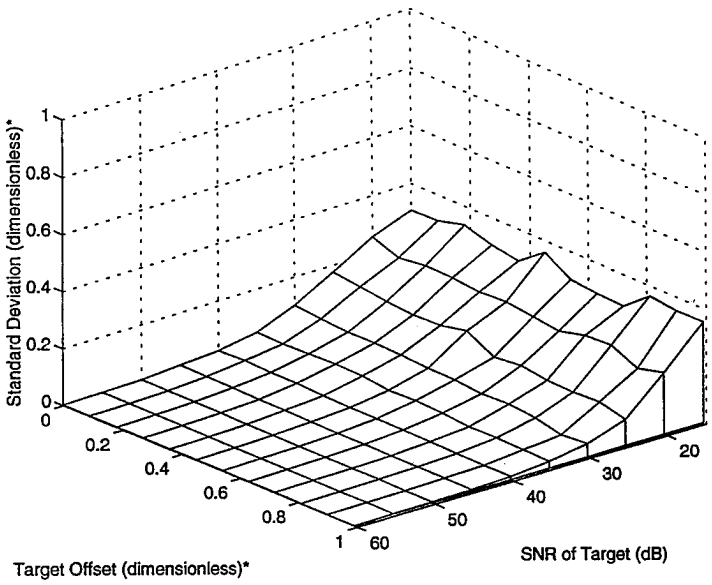

Fig. 9 — Standard deviation of azimuth estimate (*target offset and standard deviation are measured in fractions of a 3 dB beamwidth)

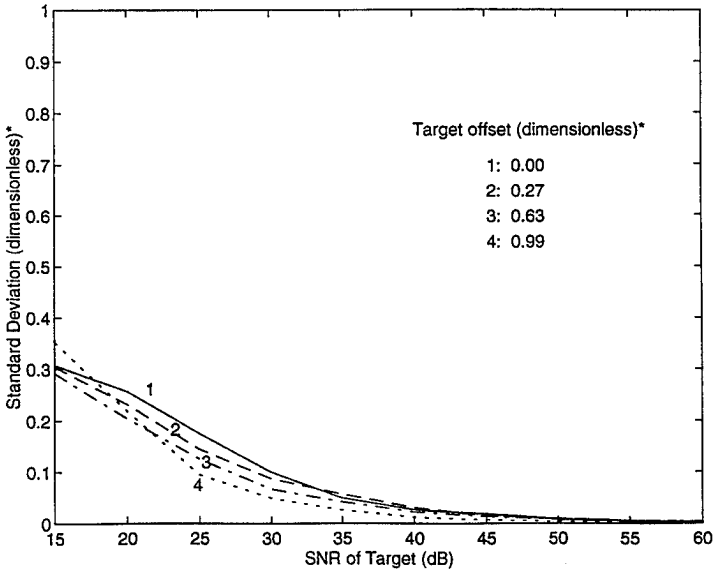

Fig. 10 — Standard deviation of azimuth estimate. These four curves have been extracted from Fig. 9 and plotted here for further clarity. (*Target offset and standard deviation are measured in fractions of a one-way 3 dB beamwidth.)

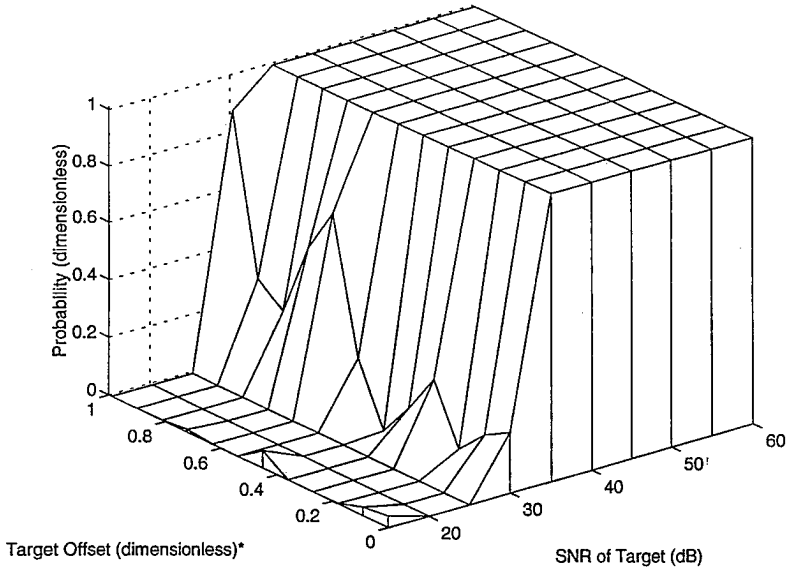

Fig. 11 — Probability that the error is less than 0.3 of a 3 dB beamwidth (*measured in fractions of a 3 dB beamwidth)

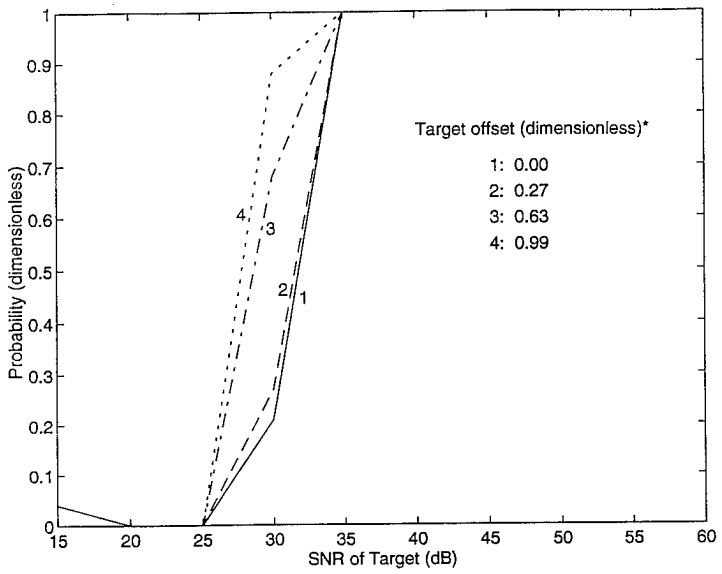

Fig. 12 — Probability that the error is less than 0.3 of a one-way 3 dB beamwidth. These four curves have been extracted from Fig. 11 and plotted here for further clarity. (*Target offset is measured in fractions of a one-way 3 dB beamwidth.)

By comparing the RMS error in Figs. 7 and 8 and the standard deviation in Figs. 9 and 10, some bias in the estimate is evident. At low SNRs, the estimate becomes more like a uniform distribution across the main lobe, which has a mean that moves closer to zero as the SNR decreases, increasing the error for targets at greater offset angles. This implies that low SNR targets at greater offset angles will, on average, have their estimates "pushed" to the center of the beam.

Table 1 — Values Used for Simulation

N	64
M	44
K	$7 \times N = 448$
windowing function	−110 dB Chebyshev
angular scan rate (α_{ant})	180°/s
antenna sampling interval (θ_s)	$0.45°/(N - 1) = 0.00714°$
main lobe beam width (to first null, as shown in Fig. 5.)	3.7°
one-way 3 dB beamwidth	1.25°

If one assumes that detections can arise from a large portion of the beam (larger than the 3 dB beamwidth), then the estimate can significantly improve the performance of the radar. In this simulation, the 3 dB beamwidth is 1.25°, but the main lobe beamwidth is about 3.7°. It is safe to assume a uniform probability distribution of detections in this main lobe, given that large targets may be encountered. The standard deviation of this distribution is 1.1° [2]. According to Fig. 7, even for a low post-integration SNR (15 dB), the estimate's error is not much worse than this $0.8 \times 1.25° = 1.0°$). Since most CFAR detectors need a threshold of at least 11 dB to maintain a low false alarm rate, enough signal power should be available to make a reasonable estimate no matter what the detection's SNR.

The chance of a detection coming from far off the 3 dB beamwidth is low unless the target is very large. In this case, the probability of detection on the next CDI is very high unless the target falls into a blind velocity or range. Using the error associated with the azimuth estimate as a sort of "gate," the tracker can cluster these two (or more) detections. Then, by weighting the azimuth estimates of the cluster by their respective SNRs and finding the average, an even more accurate estimate can be obtained.

It should be noted that this simulation assumes that the weighted echoes are generated by a point target, or a target that is small in comparison to the size of the beam. If the target were to fill a significant portion of the beam, then this algorithm may begin to break down due to the simultaneous contributions of multiple scatterers on the target. These additional contributions give rise to what is traditionally called "glint"-introduced error.

The algorithm shown in Fig. 2 may not be the most efficient way to extract the azimuth estimate from the data. For instance, there is no need to divide all K correlator outputs by the square root of the signal power as shown in Eq. (3) since only the maximum is needed to obtain the estimate. This would eliminate K divide operations. Other such improvements may be made. The algorithm presented in this report is not intended to be computationally efficient, but straightforward and, therefore, easier to understand.

SUMMARY

Greater azimuth angle measurement accuracy on a single CDI may be obtained for mechanically rotating pulse Doppler radars by a simple cross-correlation of the target echoes with a stored replica of the two-way antenna beam pattern. This estimate enhances the capabilities of the radar system in the areas of automatic tracking and track initiation. The simulation results presented here show promise of increased accuracy of the azimuth estimate even at low SNRs.

ACKNOWLEDGMENT

The authors thank Linda Schaus for use of the ambiguity diagram shown in Fig. 1.

REFERENCES

1. Simon Haykin, *An Introduction to Analog & Digital Communications* (Wiley, New York, 1989).

2. Alberto Leon-Garcia, *Probability and Random Processes for Electrical Engineering* (Addison-Wesley, Reading, MA, 1989).